frontiers in Earth Science

ORIGINAL RESEARCH
published: 22 October 2021
doi: 10.3389/feart.2021.711910

Volcanic Structures and Magmatic Evolution of the Vesteris Seamount, Greenland Basin

Katharina A. Unger Moreno[1*†], *Janis Thal*[1], *Wolfgang Bach*[1,2], *Christoph Beier*[3,4] *and Karsten M. Haase*[4]

[1]Fachbereich Geowissenschaften, Universität Bremen, Bremen, Germany, [2]MARUM Center for Marine Environmental Sciences, Universität Bremen, Bremen, Germany, [3]Department of Geosciences and Geography, Research Programme of Geology and Geophysics (GeoHel), University of Helsinki, Helsinki, Finland, [4]GeoZentrum Nordbayern, Friedrich-Alexander-Universität Erlangen-Nürnberg, Erlangen, Germany

The formation of isolated seamounts distant from active plate boundaries and mantle plumes remains unsolved. The solitary intraplate volcano Vesteris Seamount is located in the Central Greenland Basin and rises ~3,000 m above the seafloor with a total eruptive volume of ~800 km^3. Here, we present a new high-resolution bathymetry of Vesteris Seamount and a detailed raster terrain analysis, distinguishing cones, irregular volcanic ridges, volcanic debris fans, U-shaped channels and lava flows. The slope angles, ruggedness index and slope direction were combined with backscatter images to aid geologic interpretation. The new data show that the entire structure is a northeast to southwest elongated stellar-shaped seamount with an elongated, narrow summit surrounded by irregular volcanic ridges, separated by volcanic debris fans. Whole-rock geochemical data of 78 lava samples form tight liquid lines of descent with MgO concentrations ranging from 12.6 to 0.1 wt%, implying that all lavas evolved from a similar parental magma composition. Video footage from Remotely Operated Vehicle (ROV) dives shows abundant pyroclastic and hyaloclastite deposits on the summit and on the upper flanks, whereas lavas are restricted to flank cones. The seamount likely formed above a weak zone of the lithosphere possibly related to initial rifting parallel to the nearby Mohns Ridge, but the local stress field increasingly affected the structure of the volcano as it grew larger. Thus, we conclude that the evolution of Vesteris Seamount reflects the transition from deep, regional lithospheric stresses in the older structures to shallower, local stresses within the younger volcanic structures similar to other oceanic intraplate volcanoes. Our study shows how the combination of bathymetric, visual and geochemical data can be used to decipher the geological evolution of oceanic intraplate volcanoes.

Keywords: oceanic intraplate volcanism, liquid line of descent, volcanic flanks, effusive and explosive volcanism, submarine volcano morphology

OPEN ACCESS

Edited by:
Michael Stock,
Trinity College Dublin, Ireland

Reviewed by:
Wolfram Geissler,
Alfred Wegener Institute Helmholtz Centre for Polar and Marine Research (AWI), Germany
William W. Chadwick,
Hatfield Marine Science Center, Oregon State University, United States

****Correspondence:***
Katharina A. Unger Moreno
kunger@geomar.de

†Present address:
K. A. Unger Moreno,
GEOMAR Helmholtz Centre for Ocean Research Kiel, Kiel, Germany

Specialty section:
This article was submitted to Volcanology, a section of the journal Frontiers in Earth Science

Received: *19 May 2021*
Accepted: *05 October 2021*
Published: *22 October 2021*

Citation:
Unger Moreno KA, Thal J, Bach W, Beier C and Haase KM (2021) Volcanic Structures and Magmatic Evolution of the Vesteris Seamount, Greenland Basin. Front. Earth Sci. 9:711910. doi: 10.3389/feart.2021.711910

INTRODUCTION

Volcanic seamounts are abundant bathymetric features on the seafloor and are typically related to island arcs, mid-ocean ridges, and hotspot chains but also occur as solitary intraplate volcanoes (Wessel, 1997). Hotspot-related intraplate volcanoes frequently occur on relatively old and thick oceanic lithosphere and therefore the magmas represent relatively low degrees of partial melting at

high pressures resulting in alkaline, enriched compositions (Haase, 1996; Humphreys and Niu, 2009). Well-studied examples are hotspot-related seamount chains like the Hawaiian-Emperor (Regelous et al., 2003; Buchs et al., 2015) and the Louisville Seamount Chains (Lonsdale, 1988; Koppers et al., 2004). These volcanic chains are explained by plate movement across a melting anomaly formed by a thermal deep mantle plume (Morgan, 1971; Duncan and Richards, 1991). Alternative formation models for intraplate volcanism include tensional stresses which fracture the lithosphere allowing magma ascent, sub-lithospheric convection, shear-induced melting, or pre-existing zones of weakness in the lithosphere (Conrad et al., 2011; Iyer et al., 2012; Buchs et al., 2015; Gaina et al., 2017). However, numerous solitary intraplate volcanoes occur in the ocean basins (Batiza 1989; Long et al., 2020) and their formation related to plate tectonic processes is often unclear. Intraplate volcanoes commonly erupt variably evolved lavas including primitive basalts that yield insight into the composition of the upper mantle. Additionally, volatile-rich magmas may erupt explosively even at great water depth (Head and Wilson, 2003), and thus volcaniclastic rocks can be common contributors to the foundation of intraplate volcanoes (Clague et al., 1990; Helo et al., 2011).

Intraplate seamounts often show a complex morphology reflecting volcanic eruptions and mass wasting, processes that depend on the stress field of the lithosphere and/or the volcanic edifice (Fiske and Jackson, 1972; Mitchell, 2001; Schnur et al., 2017). Volcanoes taller than 3 km appear to form complex edifices, possibly because once magma reservoirs are shallow enough to occur within the volcano they may cause rift formation (Mitchell, 2001). The overall morphological structure of intraplate volcanoes can be characterized as either: volcanic-constructive or destructive erosive-depositional landforms (Grosse et al., 2009; Micallef et al., 2017; Schnur et al., 2017). Constructive as well as destructive processes take place during the periods of eruptive activity, whereas destructive processes dominate during times of quiescence and after the volcanic activity has ceased (Micallef et al., 2017). The flank morphology of volcanic seamounts reflects a combination of processes of volcanic construction and destruction including landslides, erosion, sediment deposition and tectonism (Mitchell et al., 2002; Chadwick et al., 2008, 2012).

To date, there is limited information on the initial formation and geological evolution of Vesteris Seamount which is the only solitary, large seamount in the Greenland Basin and thus may provide crucial information on the geodynamic evolution of the Greenland Basin. Here, we combine new high-resolution bathymetric, backscatter and major element geochemical data to develop a model of the volcanic and structural evolution of Vesteris Seamount in the Central Greenland Basin. We show that a combination of constructive and destructive processes shaped the volcanic edifice. The flanks of Vesteris Seamount feature a variety of volcanic ridges and volcaniclastic debris fans. Remotely Operated Vehicle (ROV) dive videos identified different effusive and eruptive eruption stages. With decreasing age, the magmatic activity focused into the structurally weak zones of the central part of the volcano. Our study demonstrates that a combination of bathymetric, observational, and geochemical data can be used to infer the evolution and growth history of solitary intraplate volcanoes distant from active plate boundaries.

GEOLOGICAL SETTING

The NE Atlantic Ocean basin started to form in the Early Eocene during the breakup of Eurasia and North America/Greenland (Torsvik et al., 2001; Garcia et al., 2012; Ellis and Stoker, 2014; Gaina et al., 2017). Magnetic isochrons show that the North Atlantic oceanic crust began forming at ~54 Ma, consistent with the oldest magnetic Chron 24 anomaly along the margins of Eurasia and Greenland (Gaina et al., 2009; Ellis and Stoker 2014). The chron's discontinuous occurrence implies that the crust was rifting instead of spreading during that period (Ellis and Stoker, 2014). The first continuous production of oceanic crust began at ~48 Ma, shown by Chron C21 (Gaina et al., 2009; Ellis and Stoker 2014). At about ~25 Ma the Aegir Ridge, the southward extension of the mid-ocean ridge (MOR) segment Mohns Ridge, became extinct and spreading started at the Kolbeinsey Ridge, due to a westward jump, south of the Jan Mayen Fracture Zone (Torsvik et al., 2001; Gernigon et al., 2012). Ellis and Stoker (2014) suggested that the final break-up took place when the Reykjanes and Kolbeinsey ridges were linked and started spreading. Oligo-Miocene plate reorganization in the North Atlantic created the final break between Greenland and Eurasia, leading to the separation of the Jan Mayen micro-continent from Greenland (Ellis and Stoker, 2014).

Vesteris Seamount is located in the Greenland Basin ~350 km east of the Greenland coastline, ~480 km west of the slow-spreading Mohns Ridge and ~250 km north of the Jan Mayen Fracture Zone (**Figure 1**). The seafloor in the Greenland Basin is generally flat and sedimented and has a depth of ~3,700 m below sea level (msbl) (Garcia et al., 2012). Several volcanic ridges extend from the NE to the SW in the Greenland Basin northeast of Vesteris Seamount (Garcia et al., 2012), but these are outcrops of old oceanic crust covered by thick Mn-crusts (Bach et al., 2019). There are no other young volcanic structures, fracture zones or transform faults in the vicinity of Vesteris Seamount and thus its origin has been enigmatic (Cherkis et al., 1994). Vesteris Seamount is hence a solitary volcanic center on 5.5 km thick and ~44 Ma old oceanic crust (Voss et al., 2009) that rises to water depths as shallow as 137 m below sea level (bsl) (**Figure 2**). The seamount is situated in an area that may be influenced by the extension of the Kolbeinsey Ridge axis to the south and the oblique spreading of the Mohns Ridge in the east (Haase and Devey, 1994). Haase and Devey (1994) suggested that the magmas formed and ascended due to fracturing of the lithosphere as a result of the combination of stresses from distant seafloor spreading. The area was previously mapped and sampled with R/V Polarstern, during expeditions ARKII/4 in 1984 and ARKVII/1 in 1990. Imagery from a photo sled indicated rich benthic ecosystems fed by a downwelling Taylor regime and dominated by sponges, bryzoans, serpulids, and echinoderms (Henrich et al., 1992). These authors also noted that the volcanic substrate was commonly covered by thick spiculite mats in the summit area of Vesteris. Uncolonized patches revealed mostly volcaniclastic sediments and different lava morphologies were exposed in escarpments. Twenty-two rock samples from eight dredge and TV-grab stations were analyzed for their major and

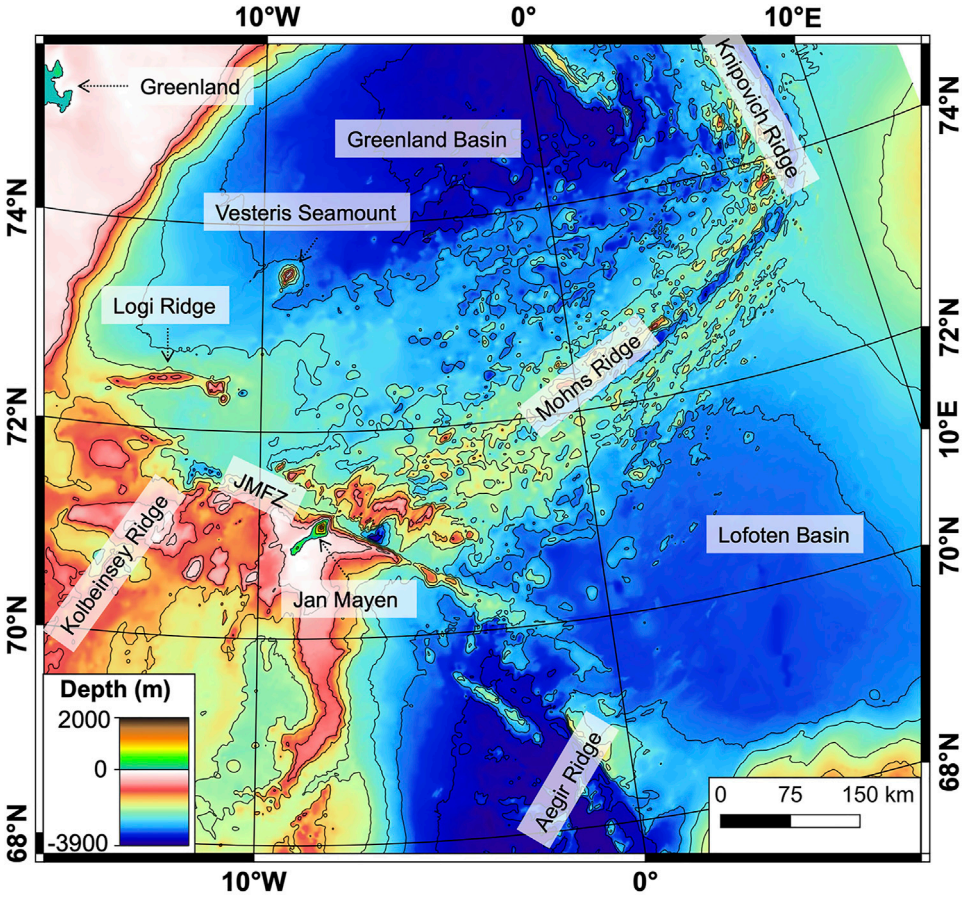

FIGURE 1 | Bathymetric map of the North Atlantic between 67 and 74.5°N showing the location of the Vesteris Seamount. The contours are 500 m elevation. All scales in the figures are linear.

trace element composition (Haase and Devey, 1994). The rocks undersaturated in SiO_2 range from alkali basalt to basanitic/tephritic in composition (Haase and Devey, 1994).

Previous work indicated that Vesteris Seamount formed episodically through multiple stages of volcanism (Mertz and Renne, 1995). Cherkis et al. (1994) suggested that the seamount has been active in Quaternary times, since there are volcanic cones on the flanks and tephra beds at shallow depth in the surrounding sediment. Argon-Ar dating of three rock samples from Vesteris Seamount showed that the trachybasalt and tephrite are 500–650 ka old and that the slightly more evolved mugearite yielded younger ages 10 to 85 ka (Mertz and Renne, 1995). Haase et al. (1996) showed that ash layers in sediment cores recovered close to Vesteris Seamount indicate numerous eruptions within the last 60 ka.

DATA COLLECTION AND SAMPLING METHODS

Bathymetric Data and Terrain Analyses

The bathymetric data presented here were obtained during expedition MSM86 on *R/V Maria S. Merian*, using the ship's two hull-mounted multibeam Kongsberg Simrad EM122 (12 kHz, deep water) and EM712 (70 kHz, shallow water) systems. Raw data were processed following a standard workflow with the open-source software package MB-System (Caress and Chayes, 1995) to obtain a high resolution bathymetric and backscatter data set. The acoustic backscatter intensity depends on the physical properties and the topography of the seafloor (Klischies et al., 2019).

The open-source geographic information system QGIS was used for geospatial data analyses and raster calculations. Two Digital Elevation Models (DEMs) with a grid-cell size of 25 and 3 m were produced to be used for raster terrain analysis which compromises the calculation of the slope angle, slope direction, hill shade, ruggedness index and relief. **Figure 2** shows a DEM with a 25 m resolution acquired by the EM122 and **Figure 3** shows a 3 m resolution DEM acquired by the EM712. The EM712 grid is smaller because it was restricted to shallow water depths less than 2,400 m bsl.

Sampling of the Volcanic Structures

Vesteris Seamount was sampled using the remotely operated vehicle (ROV) MARUM-SQUID from the Center for Marine Environmental Studies, University of Bremen, and via TV-guided

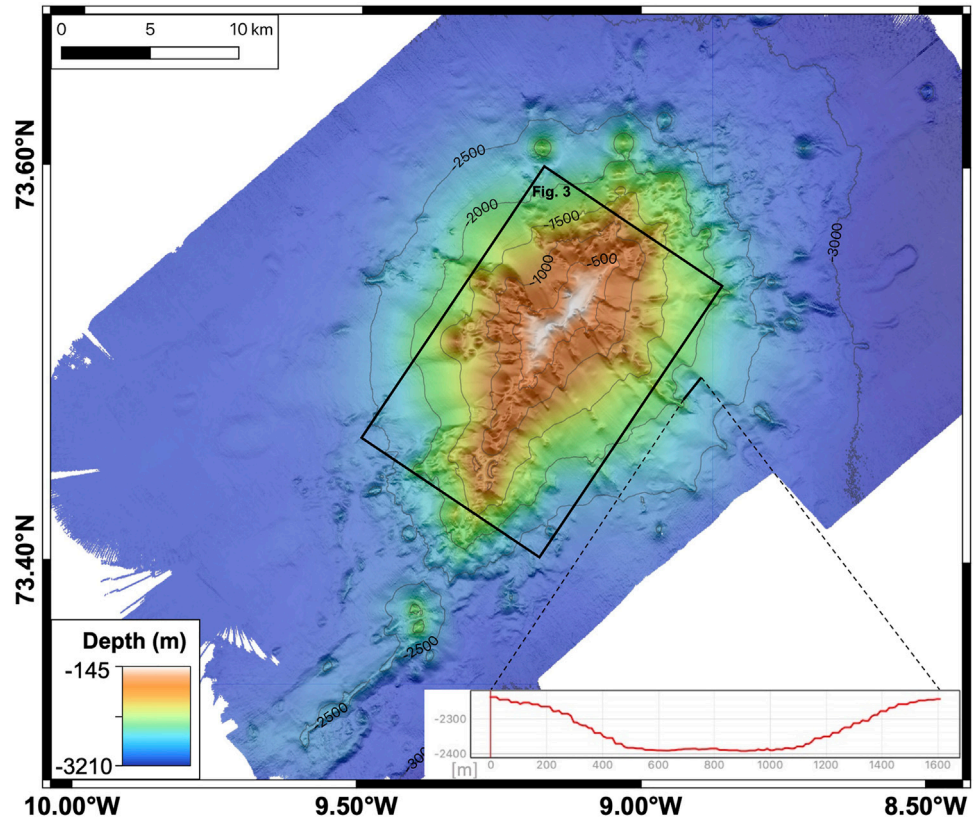

FIGURE 2 | Detailed bathymetric map of Vesteris Seamount from EM122 multibeam sonar data. The DEM has a resolution of 25 m. The inset shows a cross section of a U-shaped channel. Box shows area of **Figure 3**.

grab (TV-grab) from the GEOMAR Helmholtz-Zentrum für Ozeanforschung, Kiel. Visual observations and samples from the seamount were taken during six successful ROV dives (**Figure 3A**). We combined our new data with previously published results (Haase and Devey, 1994; Haase et al., 1996).

Geochemical Methods

A total of 78 new whole rock samples were cut, crushed, powdered and analyzed at the GeoZentrum Nordbayern, Friedrich-Alexander-Universität Erlangen-Nürnberg using a Spectro XEPOS He—XRF spectrometer previously described in Romer et al. (2018). For the whole rock analysis, 1.00 g of rock powder and 4.83 g of lithium-tetraborate ($Li_2Bi_4O_7$) were mixed and melted to prepare a homogenous glass bead. The loss on ignition was measured by heating 1.00 g of rock-powder at 1,030°C in a muffle furnace and determining the difference in weight before and after heating. The international rock standard BE-N, BR, AC-E and GA were measured to determine precision and accuracy, which are 0.8 (2σ) and 1% (2σ), respectively.

RESULTS

The newly produced geospatial data were combined with geochemical data from extensive rock sampling into a comprehensive QGIS3.10 (Version: 3.10.8) project. Volcanic facies, ROV observations and chemical compositions were combined in order to investigate the volcanic growth and stages of magmatic evolution. Classifications were made based on the morphological characteristics, the raster terrain analysis and backscatter data. For a discussion of the volcanic terrain of Vesteris Seamount, we defined several morphological features summarized in **Table 1**.

Bathymetry

The principal bathymetric features of Vesteris Seamount are depicted in **Figures 2**, **3**, and our interpretive geologic map is shown in **Figure 4**. The shallowest part of the seamount is 137 m bsl and the surrounding seafloor is 3,225 m bsl, so Vesteris Seamount rises >3,000 m above the seafloor. The volcanic edifice of Vesteris Seamount is elongated in a northeast to southwest direction, i.e., approximately parallel to Mohns Ridge (cf. **Figure 1**). The elongated appearance is due to a central ridge structure that runs through the seamount. The base of Vesteris, i.e., the transition between the abyssal plain and the constructional slopes, rather resembles an elliptical feature. Several conical peaks poke through the volcaniclastic apron on the lower flanks of the volcano (**Figure 4**). The morphology of the summit area resembles an elongated plateau with a smooth, partly undulated surface and shows

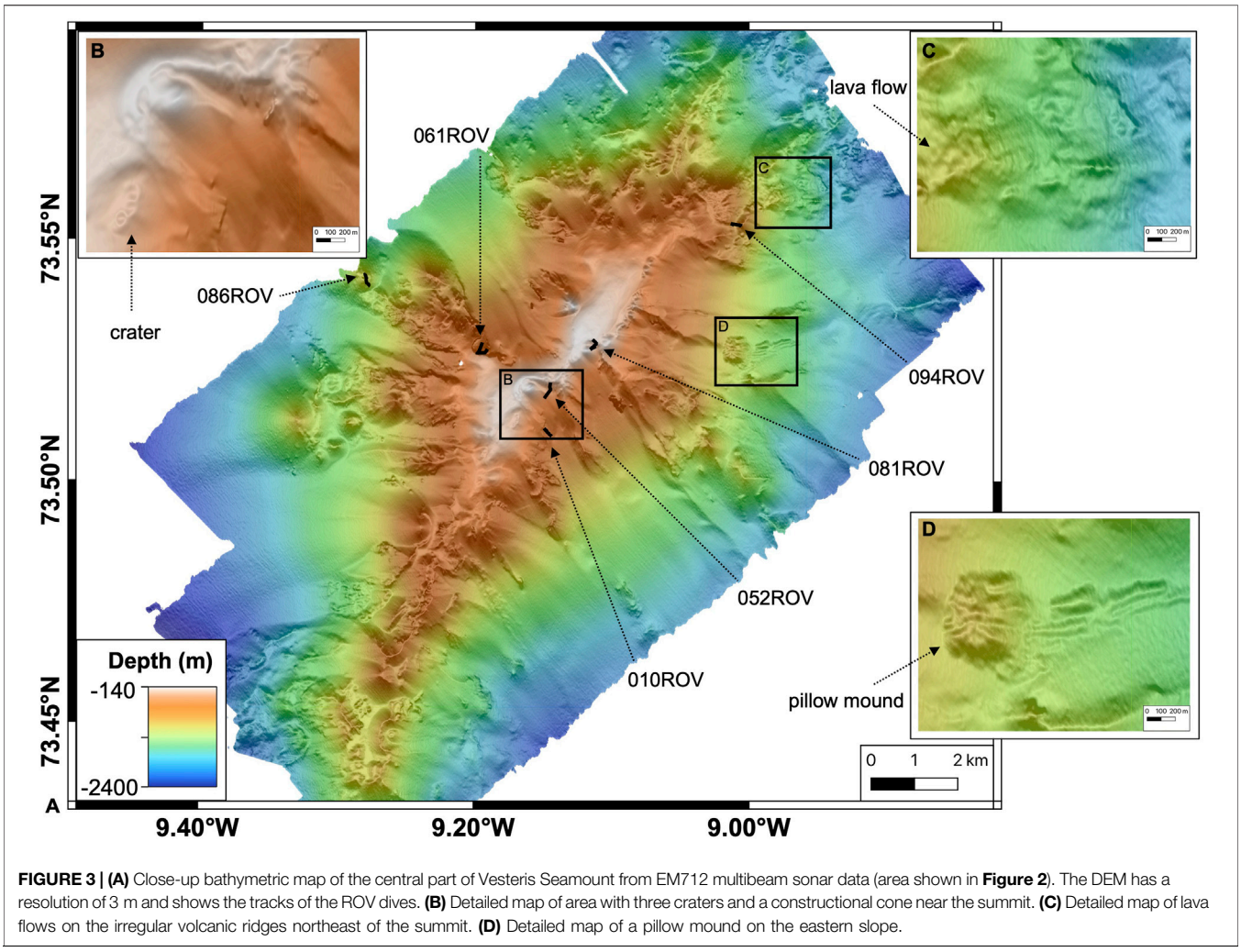

FIGURE 3 | (A) Close-up bathymetric map of the central part of Vesteris Seamount from EM712 multibeam sonar data (area shown in **Figure 2**). The DEM has a resolution of 3 m and shows the tracks of the ROV dives. **(B)** Detailed map of area with three craters and a constructional cone near the summit. **(C)** Detailed map of lava flows on the irregular volcanic ridges northeast of the summit. **(D)** Detailed map of a pillow mound on the eastern slope.

TABLE 1 | Morphological features of the Vesteris Seamount.

Units	Description
Hummocky lava flow terrain	High ruggedness index and relief, hummocky structure. Structures with a high intensity in the backscatter map
Volcaniclastic terrain	Low ruggedness index, smooth surface, flow structure in backscatter map
Volcanic cones	Conical shape, high relief and high ruggedness index
Irregular volcanic ridges	Structures which are radially oriented from the summit and main edifice
U-shaped channels	Stepwise changes in depth and ruggedness index
Summit	Smooth surface, low relief and shallow depth
Volcanic debris fan	Boundary between volcaniclastic terrain and hummocky lava flow terrain with steep slopes angles

signs of slope instability in the form of landslide scarps. The summit area extents for a length of about 6 km and is up to 1.2 km wide. It is unlike the flat-topped and icesheet-scoured seamounts of the Logi Ridge in the south (Breivik et al., 2012) and hence lacks evidence for erosion related to being above sea-level in the past. However, the abundance and massiveness of the spiculite mats may have obscured such erosional features. Along the central ridge several depressions/craters exist together with small cones (**Figure 3B**). Several head scarps near the summit area were identified. Below these head scarps debris fans show signs of mass wasting in the form of channels or a wavy, stepwise morphology which become wider towards the foot of the slopes. The flanks northwest and southeast of the central edifice of Vesteris Seamount feature small cones and ridges that strike roughly perpendicular to the summit and alternate with smooth volcanic debris fans. To the northeast and southwest the summit plateau grades into hummocky terrains with radiating irregular shaped ridges and small cones (**Figure 5**). Several large satellite cones occur in the northwestern area.

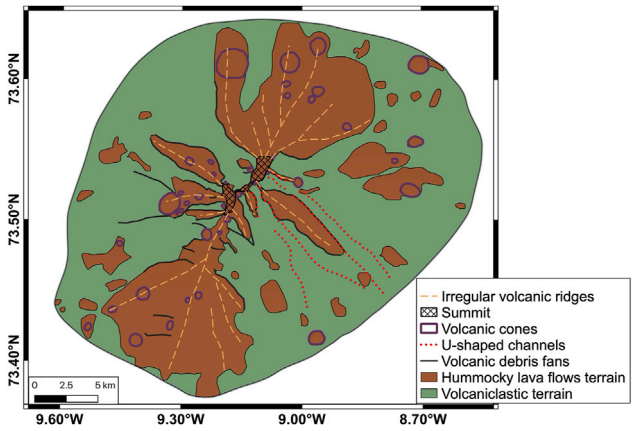

FIGURE 4 | Geological map of the Vesteris Seamount. Criteria for distinguishing between the different structures and units mapped, are provided in **Table 1**.

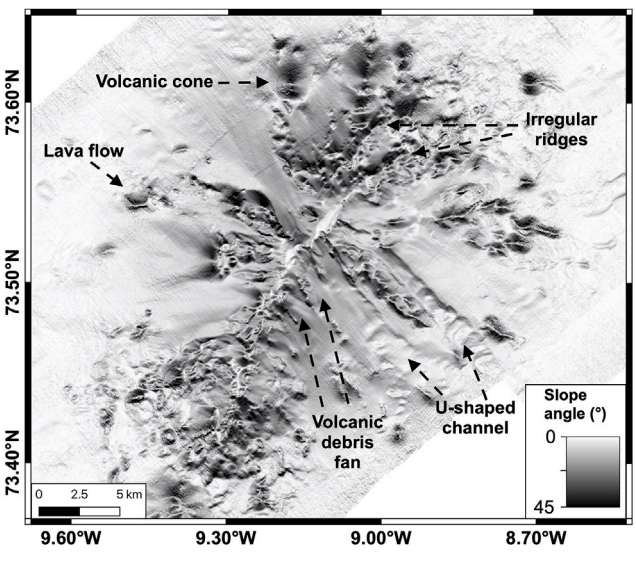

FIGURE 5 | Map of the slope angles of the Vesteris Seamount with various volcanic structures labeled.

The transition from the seamount to the surrounding regional abyssal plain is gradual. The different terrain types mapped out in **Figure 4** are accentuated by maps showing the slope angle distribution (**Figure 5**), ruggedness (**Supplementary Material**) and slope direction (**Supplementary Material**) and will be discussed in more detail in section "*Geochemical Methods*". The abyssal plain surrounding Vesteris Seamount is mostly flat, although to the northwest a channel-levee system can be recognized in the bathymetry, which has been described previously by Garcia et al. (2012). Additionally, several ridge-like features were observed on the ocean floor south of Vesteris Seamount. These ridges are also NE-SW elongated but do apparently not link up to Vesteris Seamount (**Figure 2**).

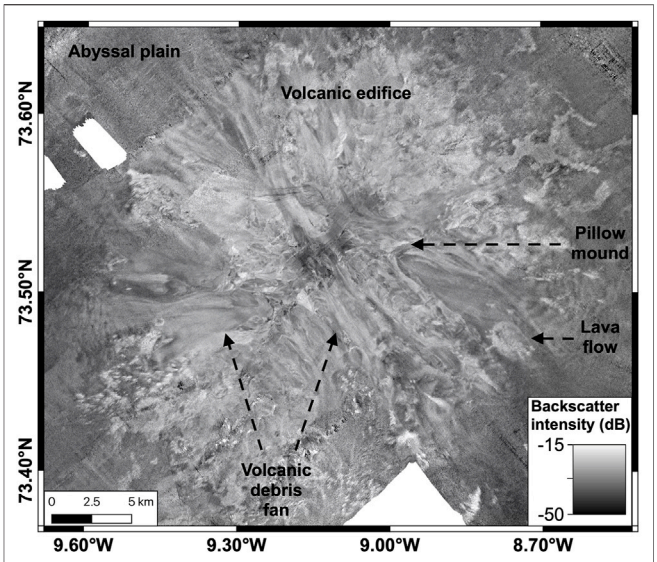

FIGURE 6 | Map of the acquired backscatter data, highlighting lava flows and volcaniclastic deposits.

Backscatter

Our new backscatter data (**Figure 6**) suggest that the low intensity volcanic features with low backscatter intensity are covered by some sediment (Eason et al., 2016; Innangi et al., 2016), whereas areas with high intensities have rough volcanic terrain (Eason et al., 2016; Innangi et al., 2016). The backscatter data help to identify the area of the seamount, which is surrounded by soft sediment of the abyssal plain. The low intensity ellipse outlining the extent of the volcano has a length of 33 km and is 27 km wide. This corresponds to an areal extent of the volcanic edifice of ~737 km^2 with an approximate volume of 800 km^3, assuming a perfect cone shape. The volcanic debris fans are characterized by variable backscatter values indicative of an uneven distribution of coarse- and fine-grained materials in the fans. Lava flows at the base of the edifice show a higher backscatter intensity compared to the surrounding terrain. The irregular ridges and cones cannot be identified in the backscatter map, except for a pillow mound (**Figure 3D**) on the eastern slope, which stands out due to its high backscatter intensity.

Morphological Characterization and Classification

For the purpose of our work, we subdivided the morphological features into two superordinate groups using differences in the ruggedness index and relief. The ruggedness index is described as the distribution of terrain heterogeneity by calculating the change in elevation between a grid cell and its 3 × 3 neighbor cells (Riley et al., 1999). A peak or pit type topography would have a greater ruggedness index than undulating topography (Riley et al., 1999). The first subordinate group is *hummocky lava flow terrain*, which are defined by a high ruggedness index, many changes in the relief, hummocky structure and some show a high backscatter intensity. The second subordinate group is *volcaniclastic terrain*;

these are characterized by a smooth surface, small slope angles (mostly below 20°) and a low ruggedness index. The *lava flows* and satellite *cones* at the base of the volcano as well as basement outcrops bordering headwalls of the slopes can be distinguished from the *volcaniclastic terrain* by having steeper slope angles up to 45°. The slopes show hummocky structures with a high ruggedness index indicating *lava flows* that are surrounded by a low ruggedness index. *Volcanic cones* on the ridges are identified by their differences in slope angle and their conical morphology. In general, the flanks of the *volcanic cones* are above 20° and their ruggedness index is above 15. These *volcanic cones* have different sizes and the largest cones are not situated on the main edifice, but surround the main edifice. *Irregular volcanic ridges* have a similar slope angles and ruggedness index as the cones but do not have a round shape, but rather display irregular elongated shapes and a hummocky structure, spreading radially from the main edifice. Slope angles exceeding 40° are developed exclusively along the headwalls and scars bordering the ridges and in areas where massive lava flows or dikes are exposed adjacent to *volcaniclastic terrain*. The edges of the ridges have steep slopes due to mass wasting. The *volcaniclastic terrains* are smoother than the volcanic structures such as *volcanic cones*, *hummocky lava flows* and *irregular volcanic ridges*; therefore, they can be distinguished from the constructional volcanic features. The *volcaniclastic terrains* on the flanks of the seamount have slopes between 8° and 21° and a ruggedness index of 5–18, smoother than the volcanic structures. They start with inclined steep slopes of up to 30° but becoming flatter with depth and level out towards the abyssal plain. The slope direction map (**Supplementary Material**) allows charting of the extent of the *volcanic debris fans*, which are defined by a narrow chute, are close to the headwall scars, and have a depositional lobe with increasing depth. The *summit* is identified by its smooth surface, inclination below 10°, low relief and shallow depth.

The occurrence of *U-shaped channels* is apparent from a low ruggedness index and a smooth surface similar to the slopes, providing evidence for sector collapses and resulting mass flows down the flanks of the seamount. The cross-sectional view of a *U-shaped channel* is shown in **Figure 2**. There are two *U-shaped channels* on the eastern flank of the seamount, one is very pronounced and terraced, and the other is smooth and apparently has been partly filled by sediments (**Figure 5**).

Overall, Vesteris Seamount has four main types of volcanic structures: 1) irregular volcanic ridges, 2) volcanic cones, 3) hummocky lava flows and 4) volcanoclastic deposits.

ROV Observations

Six dives with the ROV provide direct observations of the volcanic facies and structures of the seafloor on Vesteris Seamount, between 157 and 1,170 m bsl, but thick spiculite mats and hedges of bryozoans made geological observations and rock sampling at some stations difficult (**Figure 9E**). The different rock types were classified from the ROV video footage and the distribution of the retrieved samples. The variety of rock types range from hyaloclastites, consolidated and unconsolidated pyroclastic material, to pillow lava, blocky lava, sheet lava and lobate lava. Dive 41 (010ROV) took place on a slope southeast of the summit (**Figure 3**) from around 500 to 670 m bsl. The slope was mostly covered by pelagic sediment with lapilli on top. Some small outcrops of lava flows covered by biota were also observed. **Figure 9A** shows the lapilli-covered pelagic sediment and some rock fragments. Dive 42 (052ROV) was performed east of the summit in depths between 180 and 300 m bsl. The seafloor was covered by biota and several pieces of lapilli. A long vertical outcrop exposing layered volcaniclastic deposits was sampled, and black coarse ash and lapilli were retrieved. **Figure 9B** shows a representative outcrop of the volcaniclastic deposits. Dive 43 (061ROV) was located northwest of the summit along a steep outcrop of laminated volcaniclastic material directly beneath a ridge (**Figure 9C**). Dive 44 (081ROV) was close to the summit of Vesteris Seamount and targeted dome-like structures in water depths between 220 and 190 m bsl (**Figure 9D**) consisting of brecciated and iron-stained hyaloclastites. The surrounding seafloor was covered by spiculite mats and almost no tephra was observed. Dive 45 (086ROV) targeted a satellite volcanic cone on a ridge extending northwest of the summit at a depth of 1,170 m bsl where different lava flow morphologies are exposed on near-vertical walls and pillow lavas, sheet flows and lobate flows were observed (**Figure 9F**). Dive 46 (094ROV) was conducted in a depression within an irregular ridge in the lava flow terrain northeast of the summit. Both sides of the depression were investigated and the seafloor on both sides was similar in appearance with ropy and sheet lava outcrops (**Figures 9G,H**).

Geochemistry

The rocks sampled at Vesteris Seamount are aphyric to highly porphyritic lavas, often from pillow flows, as well as unconsolidated lapilli and bombs of pyroclastic origin. Additionally, samples of consolidated volcanic ash were recovered. Lava and coarse tephra are characterized by abundant vesicles. Mafic lavas typically contain olivine and clinopyroxene whereas plagioclase is less abundant. Most rock samples are very fresh and glass rims are abundant, but several samples are covered by a Fe-Mn oxide-hydroxide staining. The SiO_2 contents vary from 39.4 to 61.8 wt%, tending higher compared to those recovered from previous sampling (Haase and Devey, 1994). The total alkali content (Na_2O + K_2O wt%) versus SiO_2 wt% diagram (LeBas et al., 1986; **Figure 7**) shows that the majority of the samples are basanites and tephrites similar to those sampled previously, but some alkali basalts and trachybasalts do also occur. The SiO_2-richer samples range from phonotephrite and tephriphonolite to trachyandesites, phonolite and trachyte forming a continuous trend. Major element concentrations show increasing trends of Al_2O_3, Na_2O, and K_2O with decreasing MgO, whereas all other oxides display a change in slope at ~5 wt% MgO indicating changes in the fractionation assemblage (**Figure 8**). The TiO_2, Fe_2O_3, CaO, and P_2O_5 contents are either constant or increase to 5 wt% MgO and then decrease, whereas SiO_2 contents increase with decreasing MgO.

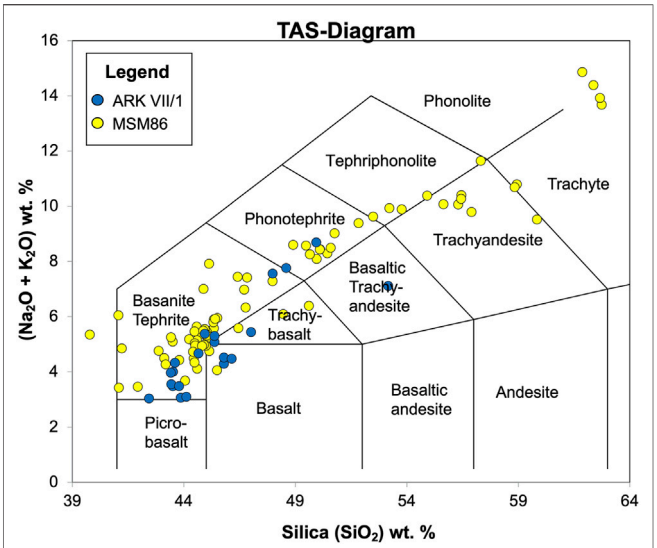

FIGURE 7 | Total Alkaline Silica-diagram; blue dots are the previously collected samples from expedition ARKVII/1 and yellow dots are the newly collected samples from expedition MSM86.

DISCUSSION

Volcanic Construction of Vesteris Seamount

The evolution of polygenetic intraplate volcanoes strongly depends on the structure and stress state of the lithosphere because magmas typically ascend in dikes that follow the regional stress orientation (Nakamura, 1977). Intraplate volcanoes often have a stellate shape reflecting the relief of radiating volcanic rift zones above dikes (Mitchell, 2001). However, an elongated structure like Vesteris Seamount (**Figure 2**) rather resembles volcanoes from extensional plate boundaries that largely follow dike swarms perpendicular to the least compressive stress σ_3 (Klügel et al., 2005; Clague et al., 2011; Romer et al., 2019). Thus, the NNE-SSW elongation of Vesteris Seamount suggests an ESE-WNW directed extension in this part of the Greenland Basin, i.e., roughly parallel to the spreading direction of 105–110° at Mohns Ridge (Dauteuil and Brun, 1993). The volcano has probably been fed by dikes ascending over its 30 km length and parallel to the NNE-SSW orientation of the volcanic edifice. Most of the lavas sampled along this main volcanic rift axis are primitive with >5 wt% MgO (**Figure 10**) suggesting that they tapped deeper parts of the magma reservoir.

The northern part of Vesteris Seamount at about 73.5°N shows several irregular ridges striking perpendicular to the main edifice (**Figure 2**) and these probably represent dike-fed ridges. **Figure 4** emphasizes that the irregular ridges are covered by lava flows (**Figure 3C**). The lava flows typically consist of pillow lavas, and less abundant sheet flows and lobate flows (**Figures 9F–H**). They probably mark the eruption sites of dikes transporting magma from the central magma plumbing systems radially outward towards the flanks. The stellate shape of intraplate volcanoes develops with increasing volcano height between 2 and 4 km and has been suggested to be related to the depth of the magma reservoir above the edifice's basement causing lateral magma flow into volcanic rift zones (Mitchell, 2001). Thus, the large size of Vesteris Seamount may have allowed formation of a shallow magma reservoir within the edifice that could feed laterally propagating radial dikes. However, evolved lavas with less than 3 wt% MgO also erupt from flank cones of Vesteris Seamount (**Figure 10**), implying that magma stagnation and differentiation occurred deeper in the crust and likely below the basement of the Vesteris edifice. The MgO contents of the lavas sampled along the dikes perpendicular to the ridge crest vary considerably (**Figure 10**), suggesting multiple intrusions and effusive eruptions along these features. We conclude that these perpendicular dikes were active over longer periods and were fed by different magma reservoirs in the crust with evolving compositions.

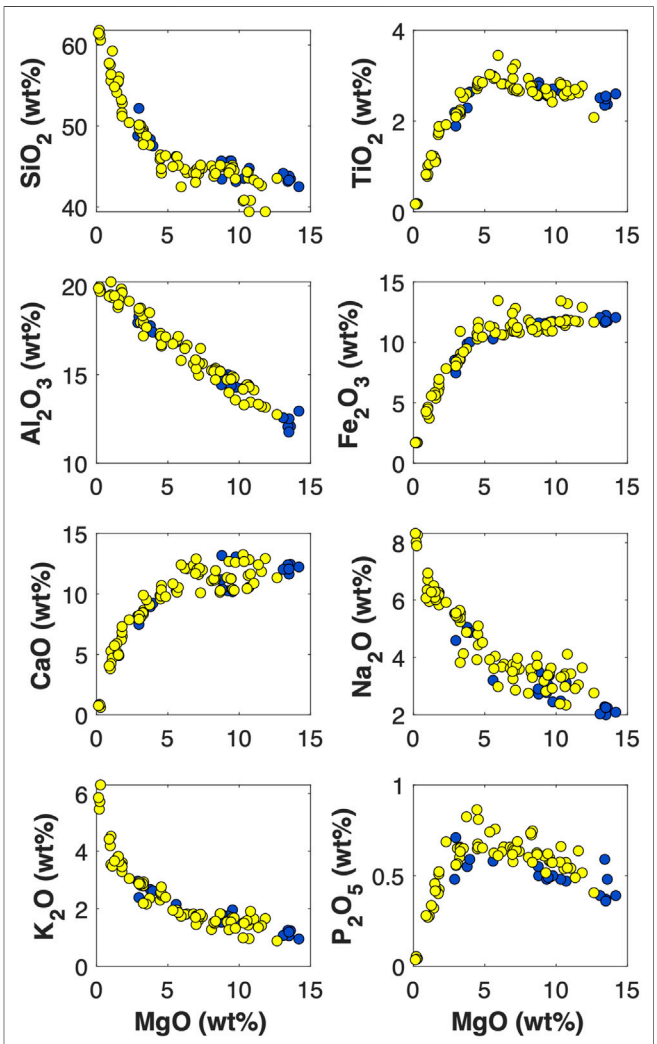

FIGURE 8 | Diagrams of MgO versus concentrations of major element oxide concentrations (Fenner-diagrams). Blue dots are the samples from expedition ARKVII/1 and displayed in yellow are the samples from MSM86.

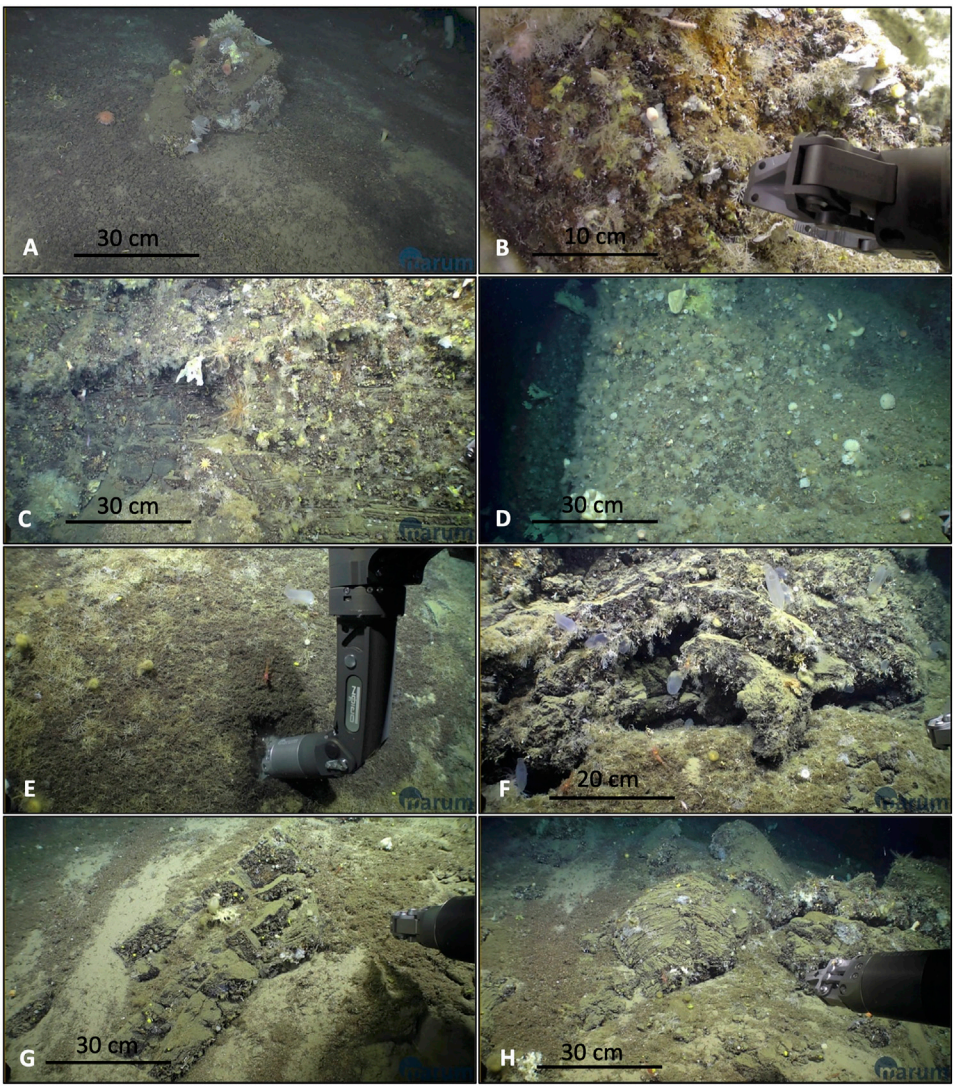

FIGURE 9 | Images of eight different facies types taken with the ROV camera system. See **Figure 2** for ROV dive locations. **(A)** Slope from 010ROV, covered by fine sediment, lapilli and rock fragments with biota. **(B)** Close up of volcaniclastic deposits during 052ROV. **(C)** Vertical wall of laminated pyroclastic material observed at 061ROV. **(D)** High wall made up of hyaloclastites at 081ROV. **(E)** Example of a slope covered by a thick spiculite mat during 086ROV. **(F)** Lobate lava from 086ROV. **(G)** Sheet lava outcrop from 094ROV. **(H)** Pillow lava with a ropy structure from 094ROV.

Vesteris Seamount shows four main types of volcanic structures: 1) irregular volcanic ridges representing dike-fed eruptions, 2) volcanic cones, 3) hummocky regions of pillow and lobate lava flows on the flanks, and 4) smooth volcaniclastic deposits on the flanks (**Figure 4**). The abundance of dike-fed rifts, volcanic cones and lava flows at the northeastern and southwestern ends of Vesteris Seamount likely reflects an effusive stage of volcano growth. The lava morphology reflects the eruption rate where lobate lavas commonly form at higher eruption rates (<10 m^3/s) compared to pillow lavas (<1 m^3/s), and the highest eruption rates result in sheet lavas (>100 m^3/s) (Gregg and Fink, 1995; McClinton and White, 2015; White et al., 2015). The lobate flows and pillow lavas observed at Vesteris Seamount thus indicate moderate eruption rates.

Binard et al. (1992) suggested three stages for intraplate volcanism growth: 1) high discharge rate of lava, 2) a succession of volcanic cones, 3) phreatic and phreatomagmatic eruptions. The effusive volcanic rocks of Vesteris Seamount then represent the early stage of volcano growth, whereas the volcaniclastic deposits at the flanks appear to be a later stage of activity and mainly fed by pyroclastic eruptions of vents at the central shallow part of the volcano. Additionally, volcanic debris from these vents has been deposited on the smooth slopes. Basanitic magmas contain high contents of CO_2 and pyroclastic basanite eruptions with large plumes in the water column were observed at water depths of <300 m bsl at El Hierro in the Canary Islands (Somoza et al., 2017). We suggest that similar

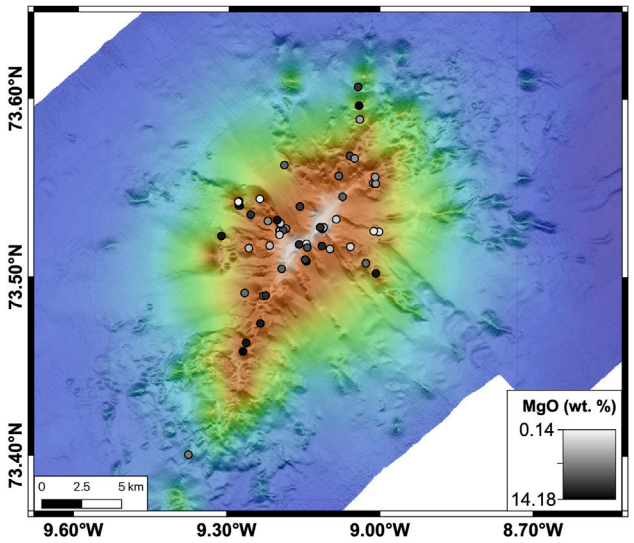

FIGURE 10 | Bathymetric map as in **Figure 2** presenting lava sample locations from cruises ARKVII/1 and MSM86. The color code indicates the MgO (wt%) of the samples.

pyroclastic eruptions formed the alignment of vents along the shallow volcanic ridge in the center of Vesteris Seamount and that these vents produced the large areas on the flanks consisting of layers of lapilli- to ash-sized material (**Figure 9C**). A conceptual model of the growth of Vesteris seamount is presented in **Figure 11**. The cartoon emphasizes the dominance of effusive activity in the early stage, common volcaniclastic eruptions during the intermediate stage and flank collapse along with summit hyaloclastite deposition in the late stage.

Destructive Mass Wasting at Vesteris Seamount

The flanks of Vesteris Seamount have irregular morphologies with extensive debris fans (**Figure 4**), indicating flank collapses (Grosse et al., 2009). Flank embayment and U-shaped slope channels (**Figure 2**) provide additional evidence for slope failure (Chaytor et al., 2007). Headwalls occur frequently close to the summit above the debris fans (**Figure 3B**) and mark landslide scars of slope failure events. The relatively smooth slopes consist of volcanic debris formed either during pyroclastic eruptions or by disintegrated lava from effusive eruptions on steep slopes as has been observed at West Mata Volcano in the NE Lau Basin (Clague et al., 2011). These slopes also have a small ruggedness index and lack of hummocks which points towards a deposit of unconsolidated volcaniclastic debris instead of mass movements of large blocks. ROV dive 43 (061ROV) footage shows steep fault scarps exposing thick layers of volcaniclastic deposits (**Figure 9C**) that likely formed by constructive, volcanic rather than destructive, erosional processes. The pyroclastic deposits are often capped by lava flows indicating alternating explosive and effusive eruptions, possibly reflecting changes in composition or gas contents of the erupting lavas.

The irregular ridges on the lower flanks of the seamount have several chutes in-between. Early flank collapses are covered by pyroclastic material from later volcanic activity. This can be observed on the southeastern flank where a U-shaped channel is almost buried by later volcanic debris fan infills (**Figure 2**). The prominent irregular ridges at the main edifice of Vesteris Seamount are either remnant dikes and lava flows exposed after the collapse of the volcaniclastic deposits, or they may be later flank eruptions that were not completely covered by debris chutes. Similar remnant outcrops were described by Chadwick et al. (2005) at the Anatahan Volcano, in the central Mariana volcanic arc. In the backscatter map these lava flows have a higher

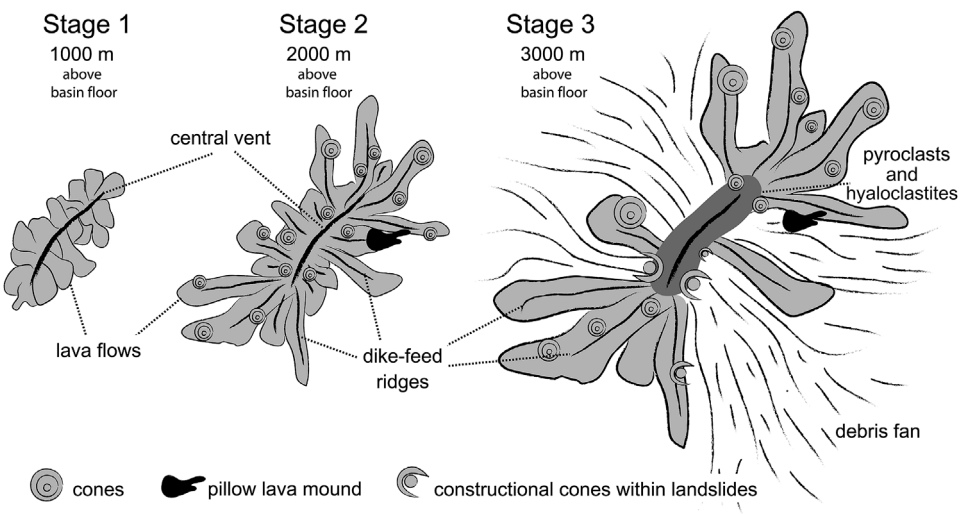

FIGURE 11 | Interpretive Cartoon illustrating three volcanic growth stages of Vesteris Seamount.

intensity than the surrounding terrain, which indicates less sediment coverage. The stellar shape of Vesteris Seamount results from the formation of the embayments between the ridges and reflects its evolution by sector collapse of the unconsolidated volcaniclastic deposits changing the volcano's shape over time.

One of the most common triggering factors for sector collapses are magma emplacement processes (Acocella, 2005). Several vents occur along the shallow central ridge of Vesteris Seamount above the collapse scars and display the characteristics of constructional cones within landslide scars (**Figure 3B**). Such cones have a similar structure to other vents on Vesteris Seamount but have grown within a half-round amphitheatre-like structure formed by previous landslide events (Chaytor et al., 2007). The cones have formed within an arcuate embayment which represents a landslide headwall. The sector collapse is likely due to 1) oversteepening of volcaniclastic material, 2) intrusions, or 3) failure of weak or altered layers beneath (Chadwick et al., 2008). The association of headwalls of the slide scars at Vesteris Seamount with eruptive vents suggests it is likely that volcanic overloading occurred (cf. Chadwick et al., 2008). Frequently, new eruptive cones formed within these slide scars above structural weak zones (**Figure 3B**). Experimental work by Acocella (2005) showed that volcanic loading could produce slide scars at the summit, which are narrow and shallow. The deposits below the collapse are smooth and have a low ruggedness index, which indicates that they mostly consist of volcaniclastic material. These are indicators for a deposit of unconsolidated volcaniclastic debris rather than flank collapse of large blocks derived from massive lava flows. Volcaniclastic material on the slope was observed at 061ROV dive (**Figure 9C**), showing exposures of laminated deposits below the summit. Hyaloclastites are created by hydromagmatic eruptions, as the seamount grows towards shallower water depths (Staudigel and Schmincke, 1984). The hyaloclastites found on the summit and at eruption vents of Vesteris Seamount (**Figure 9D**) represent pyroclastic deposits of the youngest growth stage. The overall volcanic structure of Vesteris Seamount resembles that of West Mata Volcano in the NE Lau Basin (Clague et al., 2011; Resing et al., 2011; Chadwick et al., 2019) with flanks consisting of volcaniclastic and lava debris and the rift zone being built by lava plateaus, showing that rift eruptions tend to be effusive (Clague et al., 2011). Such a structure is also observed at Vesteris Seamount (**Figure 4**), the flanks west and east are characterized by chutes and the NE-SW rift zones are constructed by hummocky ridges of effusive volcanic rocks. We conclude that volcanoes erupting volatile-rich lavas in extensional regions follow similar processes of construction and destruction due to the fact that volatile-rich eruptions mainly consist of volcaniclastic material, which is more likely to be affected by erosion.

Magmatic Evolution of Vesteris Seamount

The magmas at Vesteris Seamount may have formed by partial melting of metasomatically enriched mantle (Storey et al., 2004) or northward-directed mantle flow from Kolbeinsey Ridge (Breivik et al., 2008). Alternatively, the extensional regional stresses may lead to dilation of the lithosphere allowing ascent of magmas from the low velocity zone (Haase and Devey, 1994). The major element compositions of the new samples indicate that the magmas at Vesteris Seamount follow a tight trend of fractional crystallization, in which the fractionation assemblage is dominated by olivine and clinopyroxene from the primary magmas at ~12 wt% MgO to ~5 wt% MgO. At MgO contents of <5 wt% the fractionation assemblage is dominated by clinopyroxene, Fe-Ti oxides, and apatite. Similar trends have previously been observed at the Sete Cidades Volcano, São Miguel, Azores (Beier et al., 2006) and imply that the magmas evolve along a single liquid line of descent. The most mafic lavas occur both along the central vent and along the ridges and cones, whereas lavas with MgO <3 wt% are restricted to the ridges east and west of the main edifice (**Figure 10**). We propose that all magmas at Vesteris Seamount continuously fractionated in a single central magma reservoir system that was active throughout the lifetime of the volcano and starting at least 650–10 ka (Mertz and Renne, 1995).

The occurrence of evolved lavas at the ridges east and west of the summit area suggests that the younger eruptions may be restricted to the central edifice, i.e., with decreasing age, the magmatic activity focusses into the structural weak zones of the central vent. A basaltic trachyandesite (mugearite), a trachybasalt and a tephrite from expedition ARK VII/1 have been age-dated by Mertz and Renne (1995); they were recovered from a ridge flank in the west from a water depth of <550 m bsl. Of the three samples, the mugearite has the youngest age (0.05 ± 0.02 Ma), while the other two rocks gave ages around 0.5 and 0.6 Ma. The mugearite is the most evolved rock (3.0 wt% MgO; Haase and Devey, 1994) of the published, age-dated samples. This may indicate that the evolved lavas occur relatively late in the eruption sequence. We also note that most of the sampled lavas with <2 wt% MgO occur on the deep flanks of Vesteris Seamount, which may indicate that they tap reservoirs (possibly sills) at the cool edge of the magma plumbing system (cf. **Figure 10**).

Vesteris Seamount Volcanism as a Possible Precursor of Lithospheric Rifting

Vesteris Seamount is a solitary volcano without any nearby large-scale plate boundary and is not associated with Jan Mayen or MOR volcanism (Haase and Devey, 1994; Mertz and Renne, 1995). Tectonic stresses define the pathways of ascending melts in the lithosphere and thus often control the morphology of the volcanic structure (Nakamura, 1977). The geodynamic positioning of Vesteris Seamount far from other intraplate volcanoes and divergent plate boundaries allows us to interpret the evolutionary processes of the seamount as a solitary structure. Vesteris Seamount shows a pronounced elongation roughly parallel to the Mohns Ridge. This elongated structure indicates that the volcano was governed by feeder dikes (Iyer et al., 2012) whose orientation was influenced by regional extensional stress, thus forming a ridge-like structure. Thus, the structure of Vesteris Seamount is similar to those of West Mata Volcano in an extensional rear-arc basin (Clague et al., 2011) and Davidson seamount in the eastern Pacific (Clague et al.,

2009). Extensional lithospheric stress typically causes formation of graben structures along normal faults but no depressions parallel to Vesteris Seamount are observed (**Figure 2**). Garcia et al. (2012) suggested that young volcanic structures occur north of Vesteris Seamount, but our observations and sampling of these bathymetric highs revealed mafic to ultramafic rocks with thick Mn-crusts, implying old tectonic features (Bach et al., 2019). Additionally, there is no seismic activity in the region of Vesteris Seamount (Gaina et al., 2017) that would indicate recent normal faulting. However, little is known about the initial processes of ridge jumps in the ocean basins and one model suggests that magmatic activity of a melting anomaly in the mantle is required to heat the lithosphere prior to rifting (Mittelstaedt et al., 2008). Consequently, the extensive volcanic structure of Vesteris Seamount may represent an early stage of rifting of the lithosphere of the Greenland Basin, possibly preceding a ridge jump from Mohns Ridge to the west similar to the jump from Aegir Ridge to Kolbeinsey Ridge 25 million years ago (Brandsdottir et al., 2015).

SUMMARY AND CONCLUSION

Vesteris Seamount was surveyed by ship-based multibeam sonar and sampled by ROV and TV-grab during the *RV Maria S. Merian* expedition MSM86 in 2019. A raster terrain analysis of the DEM of the Vesteris Seamount was used to identify different morphological features (**Table 1**). Parameters such as slope angle, ruggedness index and slope direction were combined with the backscatter map and geochemical data to assist in mapping the extent of the geologic units. We interpret Vesteris Seamount as a solitarily intraplate seamount that formed above an elongated ridge structure, that runs parallel to the Mohns Ridge. During the volcano's early constructional phase, the regional stress field generated a northeast-southwest-striking volcanic ridge erupting mainly mafic lavas. Later, this northeast-southwest-striking ridge evolved into a series of along and across-cutting ridges reflecting an increasingly complex local stress field around the volcano. The ridges likely reflect the intrusion of dikes and the eruption of evolved lavas at the seamount's flanks are the result of a temperature and compositional gradient in the magma storage system underlying the volcano. The occurrence of lavas with evolved compositions on the deeper flanks of Vesteris Seamount suggests that the magma reservoir is deeper than the base of the volcano and is consistent with decreasing temperatures towards the sides of the magma plumbing system. The occurrence of constructional volcanic features both on the flanks and in the central summit area suggests that volcanism was widespread during the constructive phase. The present morphology of Vesteris is characterized by the interaction of both constructional and landslide processes. We hypothesize that the increasing occurrence of younger eruptions in the central area and the later modification by destructive processes were probably the result of a decreasing supply of magma. Age-dating of some of the samples presented here is needed to further test this hypothesis. We suggest that Vesteris Seamount is a prime example of a large seamount growing above a lithospheric weak zone, which could be interpreted as an early indicator for a westward ridge jump of the Mohns Ridge. The initial formation of Vesteris Seamount was the result of deep, regional lithospheric stresses, whereas the current morphology of Vesteris is dominated by the local stress field within the volcanic edifice.

DATA AVAILABILITY STATEMENT

The original contributions presented in the study are included in the article/**Supplementary Material**, further inquiries can be directed to the corresponding author.

AUTHOR CONTRIBUTIONS

KM carried out the work on the bathymetric data, prepared the rock samples, and drafted the manuscript. JT supervised KM and helped with data analyses and design of the figures. WB and KH designed the study. WB and CB directed the field work. All authors contributed to evaluation and discussion of the data and the writing of the manuscript.

ACKNOWLEDGMENTS

We acknowledge the help of the Foreign Office in Berlin and the Leitstelle Deutsche Forschungsschiffe in Hamburg in achieving the research permission and scheduling the cruise. We thank Captain Ralf Schmidt and his crew for their help in carrying out a successful cruise and for the pleasant and professional atmosphere on RV MARIA S. MERIAN during sometimes challenging conditions. We acknowledge the help and support of the captain and crew of MSM86 also during the ROV and TV-grab operations. We are particularly grateful to A. Strack and L. Kramer for conducting the echosounding survey and doing the initial data processing. We thank N. Nowald and the MARUM-SQUID Team and E. Fabrizius for their help and support in obtaining the sample material. WB and CB thank B. Lumsden for inspirational support. The constructive comments of two reviewers considerably improved the quality of this work. We thank the Senatskomission für Ozeanographie of the Deutsche Forschungsgemeinschaft (DFG) for funding of the cruise.

SUPPLEMENTARY MATERIAL

The Supplementary Material for this article can be found online at: https://www.frontiersin.org/articles/10.3389/feart.2021.711910/full#supplementary-material

REFERENCES

Acocella, V. (2005). Modes of Sector Collapse of Volcanic Cones: Insights from Analogue Experiments. *J. Geophys. Res. Solid Earth* 110 (B2), 1–19. doi:10.1029/2004JB003166

Bach, W., Beier, C., Peckmann, J., Bauer, J., Birgel, D., Caraite, I., et al. (2019). *RV Maria S Merian Report Vesteris Seamount*. Universität Bremen.

Batiza, R. (1989). "Petrology and Geochemistry of Eastern Pacific Spreading Centers," in *The Eastern Pacific Ocean and Hawaii*. Editors E. L. Winterer, D. M. Hussong, and R. W. Decker (Boulder, Colorado: Geological Society of America).

Beier, C., Haase, K. M., and Hansteen, T. H. (2006). Magma Evolution of the Sete Cidades Volcano, São Miguel, Azores. *Azores. J. Petrol.* 47 (7), 1375–1411. doi:10.1093/petrology/egl014

Binard, N., Hékinian, R., and Stoffers, P. (1992). Morphostructural Study and Type of Volcanism of Submarine Volcanoes over the Pitcairn Hot Spot in the South Pacific. *Tectonophysics* 206 (3-4), 245–264. doi:10.1016/0040-1951(92)90379-K

Brandsdottir, B., Hooft, E., Mjelde, R., and Murai, Y. (2015). Origin and Evolution of the Kolbeinsey Ridge and Iceland Plateau, N-Atlantic. *Geochem. Geophys. Geosyst.* 16, 612–634. doi:10.1002/2014GC005540

Breivik, A. J., Faleide, J. I., Mjelde, R., and Atlantic, N. E. (2008). Neogene Magmatism Northeast of the Aegir and Kolbeinsey Ridges, NE Atlantic: Spreading ridge-mantle Plume Interaction? *Geochem. Geophys. Geosyst.* 9 (2), a–n. doi:10.1029/2007GC001750

Breivik, A. J., Mjelde, R., and Frasetto, A. (2012). *Geophysical Survey of the Eggvin Bank and Logi Ridge - Greenland Sea. AGU Fall Meeting Abstracts T31B-2598*. American Geophysical Union.

Buchs, D. M., Hoernle, K., and Grevemeyer, I. (2015). *"Seamounts", in Encyclopedia of Marine Geosciences*. Heidelberg: Springer, 1–11.

Caress, D. W., and Chayes, D. N. (1995). "New Software for Processing Sidescan Data from Sidescan-Capable Multibeam Sonars," in Challenges of Our Changing Global Environment. Conference Proceedings. OCEANS'95 MTS/IEEE., San Diego, CA, USA, 9-12 Oct. 1995, 2, 997–1000.

Chadwick, W. W., Jr, Dziak, R. P., Haxel, J. H., Embley, R. W., and Matsumoto, H. (2012). Submarine Landslide Triggered by Volcanic Eruption Recorded by *In Situ* Hydrophone. *Geology* 40 (1), 51–54. doi:10.1130/G32495.1

Chadwick, W. W., Jr, Embley, R. W., Johnson, P. D., Merle, S. G., Ristau, S., and Bobbitt, A. (2005). The Submarine Flanks of Anatahan Volcano, Commonwealth of the Northern Mariana Islands. *J. Volcanol. Geotherm. Res.* 146 (1- 3), 8–25. doi:10.1016/j.jvolgeores.2004.11.032

Chadwick, W. W., Jr, Rubin, K. H., Merle, S. G., Bobbitt, A. M., Kwasnitschka, T., and Embley, R. W. (2019). Recent Eruptions between 2012 and 2018 Discovered at West Mata Submarine Volcano (NE Lau Basin, SW Pacific) and Characterized by New Ship, AUV, and ROV Data. *Front. Mar. Sci.* 6, 495. doi:10.3389/fmars.2019.00495

Chadwick, W. W., Jr, Wright, I. C., Schwarz-Schampera, U., Hyvernaud, O., Reymond, D., and De Ronde, C. E. J. (2008). Cyclic Eruptions and Sector Collapses at Monowai Submarine Volcano, Kermadec Arc: 1998-2007. *Geochem. Geophys. Geosyst.* 9 (10), a–n. doi:10.1029/2008GC002113

Chaytor, J. D., Keller, R. A., Duncan, R. A., and Dziak, R. P. (2007). Seamount Morphology in the Bowie and Cobb Hot Spot Trails, Gulf of Alaska. *Geochem. Geophys. Geosyst.* 8 (9), 1–26. doi:10.1029/2007GC001712

Cherkis, N. Z., Steinmetz, S., Schreiber, R., Thiede, J., and Theiner, J. (1994). Vesteris Seamount: An enigma in the Greenland Basin. *Mar. Geophys. Res.* 16 (4), 287–301. doi:10.1007/BF01224746

Clague, D. A., Holcomb, R. T., Sinton, J. M., Detrick, R. S., and Torresan, M. E. (1990). Pliocene and Pleistocene Alkalic Flood Basalts on the Seafloor North of the Hawaiian Islands. *Earth Planet. Sci. Lett.* 98, 175–191. doi:10.1016/0012-821X(90)90058-6

Clague, D. A., Paduan, J. B., Caress, D. W., Thomas, H., Chadwick, W. W., Jr, and Merle, S. G. (2011). Volcanic Morphology of West Mata Volcano, NE Lau Basin, Based on High-Resolution Bathymetry and Depth Changes. *Geochem. Geophys. Geosyst.* 12 (11), a–n. doi:10.1029/2011GC003791

Clague, D. A., Paduan, J. B., Duncan, R. A., Huard, J. J., Davis, A. S., Castillo, P. R., et al. (2009). Five Million Years of Compositionally Diverse, Episodic Volcanism: Construction of Davidson Seamount Atop an Abandoned Spreading Center. *Geochem. Geophys. Geosyst.* 10 (12), a–n. doi:10.1029/2009GC002665

Conrad, C. P., Bianco, T. A., Smith, E. I., and Wessel, P. (2011). Patterns of Intraplate Volcanism Controlled by Asthenospheric Shear. *Nat. Geosci.* 4 (5), 317–321. doi:10.1038/ngeo1111

Dauteuil, O., and Brun, J.-P. (1993). Oblique Rifting in a Slow-Spreading Ridge. *Nature* 361, 145–148. doi:10.1038/361145a0

Duncan, R. A., and Richards, M. A. (1991). Hotspots, Mantle Plumes, Flood Basalts, and True Polar Wander. *Rev. Geophys.* 29, 31–50. doi:10.1029/90RG02372

Eason, D. E., Dunn, R. A., Canales, J. P., and Sohn, R. A. (2016). Segment-Scale Variations in Seafloor Volcanic and Tectonic Processes from Multibeam Sonar Imaging, Mid-Atlantic Ridge Rainbow Region (358450– 368350N). *Geochem. Geophys. Geosyst.* 17, 3560–3579. doi:10.1002/2016GC006433

Ellis, D., and Stoker, M. S. (2014). The Faroe-Shetland Basin: A Regional Perspective from the Paleocene to the Present Day and its Relationship to the Opening of the North Atlantic Ocean. *Geol. Soc. Lond. Spec. Publications* 397 (1), 11–31. doi:10.1144/SP397.1

Fiske, R. S., and Jackson, E. D. (1972). Orientation and Growth of Hawaiian Volcanic Rifts: the Effect of Regional Structure and Gravitational Stresses. *Proc. R. Soc. Lond. A.* 329, 299–326. doi:10.1098/rspa.1972.0115

Gaina, C., Blischke, A., Geissler, W. H., Kimbell, G. S., and Erlendsson, Ö. (2017). Seamounts and Oceanic Igneous Features in the NE Atlantic: A Link between Plate Motions and Mantle Dynamics. *Geol. Soc. Lond. Spec. Publications* 447 (1), 419–442. doi:10.1144/SP447.6

Gaina, C., Gernigon, L., and Ball, P. (2009). Palaeocene-Recent Plate Boundaries in the NE Atlantic and the Formation of the Jan Mayen Microcontinent. *J. Geol. Soc.* 166 (4), 601–616. doi:10.1144/0016-76492008-112

García, M., Dowdeswell, J. A., Ercilla, G., and Jakobsson, M. (2012). Recent Glacially Influenced Sedimentary Processes on the East Greenland continental Slope and Deep Greenland Basin. *Quat. Sci. Rev.* 49, 64–81. doi:10.1016/J.QUASCIREV.2012.06.016

Gernigon, L., Gaina, C., Olesen, O., Ball, P. J., Péron-Pinvidic, G., and Yamasaki, T. (2012). The Norway Basin Revisited: From Continental Breakup to Spreading Ridge Extinction. *Mar. Pet. Geology* 35 (1), 1–19. doi:10.1016/j.marpetgeo.2012.02.015

Gregg, T. K. P., and Fink, J. H. (1995). Quantification of Submarine Lava-Flow Morphology through Analog Experiments. *Geology* 23 (1), 73–76. doi:10.1130/0091-7613(1995)023<0073:QOSLFM>2.3.CO;2

Grosse, P., de Vries, B. V. W., Petrinovic, I. A., Euillades, P. A., and Guillermo, E. A. (2009). Morphometry and Evolution of Arc Volcanoes. *Geology* 37 (7), 651–654. doi:10.1130/G25734A.1

Haase, K. M., and Devey, C. W. (1994). The Petrology and Geochemistry of Vesteris Seamount, Greenland Basin--an Intraplate Alkaline Volcano of Non-Plume Origin. *J. Petrol.* 35 (2), 295–328. doi:10.1093/petrology/35.2.295

Haase, K. M., Hartmann, M., and Wallrabe-Adams, H. J. (1996). The Geochemistry of Ashes from Vesteris Seamount, Greenland Basin: Implication for the Evolution of an Alkaline Volcano. *J. Volcanol. Geotherm. Res.* 70, 1–19. doi:10.1016/0377-0273(95)00059-3

Haase, K. M. (1996). The Relationship between the Age of the Lithosphere and the Composition of Oceanic Magmas: Constraints on Partial Melting, Mantle Sources and the Thermal Structure of the Plates. *Earth Planet. Sci. Lett.* 144, 75–92. doi:10.1016/0012-821X(96)00145-8

Head, J. W., and Wilson, L. (2003). Deep Submarine Pyroclastic Eruptions: Theory and Predicted Landforms and Deposits. *J. Volcanol. Geotherm. Res.* 121, 155–193. doi:10.1016/S0377-0273(02)00425-0

Helo, C., Longpré, M.-A., Shimizu, N., Clague, D. A., and Stix, J. (2011). Explosive Eruptions at Mid-Ocean Ridges Driven by CO2-Rich Magmas. *Nat. Geosci.* 4, 260–263. doi:10.1038/ngeo1104

Henrich, R., Hartmann, M., Reitner, J., Schäfer, P., Freiwald, A., Steinmetz, S., et al. (1992). Facies Belts and Communities of the Arctic Vesterisbanken Seamount (Central Greenland Sea). *Facies* 27 (1), 71. doi:10.1007/BF02536805

Humphreys, E. R., and Niu, Y. (2009). On the Composition of Ocean Island Basalts (OIB): The Effects of Lithospheric Thickness Variation and Mantle Metasomatism. *Lithos* 112, 118–136. doi:10.1016/j.lithos.2009.04.038

Innangi, S., Passaro, S., Tonielli, R., Milano, G., Ventura, G., and Tamburrino, G. (2016). Seafloor Mapping Using High-Resolution Multibeam Backscatter: The

Palinuro Seamount (Eastern Tyrrhenian Sea). *J. Maps* 12 (5), 736–746. doi:10.1080/17445647.2015.1071719

Iyer, S. D., Mehta, C. M., Das, P., and Kalangutkar, N. G. (2012). Seamounts–Characteristics, Formation, Mineral Deposits and Biodiversity. *Geol. Acta* 10 (3), 295–308. doi:10.1344/105.000001758

Klischies, M., Petersen, S., and Devey, C. W. (2019). Geological Mapping of the Menez Gwen Segment at 37° 50′ N on the Mid-Atlantic Ridge: Implications for Accretion Mechanisms and Associated Hydrothermal Activity at Slow-Spreading Mid-Ocean Ridges. *Mar. Geol.* 412, 107–122. doi:10.1016/j.margeo.2019.03.012

Klügel, A., Walter, T. R., Schwarz, S., and Geldmacher, J. (2005). Gravitational Spreading Causes En-Echelon Diking along a Rift Zone of Madeira Archipelago: An Experimental Approach and Implications for Magma Transport. *Bull. Volcanology* 68, 37–46. doi:10.1007/s00445-005-0418-6

Koppers, A. A. P., Duncan, R. A., and Steinberger, B. (2004). Implications of a Nonlinear40Ar/39Ar Age Progression along the Louisville Seamount Trail for Models of Fixed and Moving Hot Spots. *Geochem. Geophys. Geosyst.* 5 (6), 1–22. doi:10.1029/2003GC000671

Le Bas, M. L., Maitre, R. L., Streckeisen, A., and Zanettin, B. (1986). A Chemical Classification of Volcanic Rocks Based on the Total Alkali-Silica Diagram. *J. Petrol.* 27 (3), 745–750. doi:10.1093/petrology/27.3.745

Long, X., Geldmacher, J., Hoernle, K., Hauff, F., Wartho, J. A., and Garbe-Schönberg, C. D. (2020). Origin of Isolated Seamounts in the Canary Basin (East Atlantic): The Role of Plume Material in the Origin of Seamounts Not Associated with Hotspot Tracks. *Terra Nova* 32 (5), 390–398. doi:10.1111/ter.12468

Lonsdale, P. (1988). Geography and History of the Louisville Hotspot Chain in the Southwest Pacific. *J. Geophys. Res. Solid Earth* 93 (B4), 3078–3104. doi:10.1029/JB093iB04p03078

McClinton, J. T., and White, S. M. (2015). Emplacement of Submarine Lava Flow fields: A Geomorphological Model from the Niños Eruption at the Galápagos Spreading Center. *Geochem. Geophys. Geosyst.* 16, 899–911. doi:10.1002/2014GC005632

Mertz, D. F., and Renne, P. R. (1995). Quarternary Multi-Stage Alkaline Volcanism at Vesteris Seamount (Norwegian—Greenland Sea): Evidence from Laser Step Heating 40Ar/39Ar Experiments. *J. Geodyn.* 19 (1), 79–95. doi:10.1016/0264-3707(94)E0001-B

Micallef, A., Krastel, S., and Savini, A. (2017). *Submarine Geomorphology*. Cham, Switzerland: Springer. doi:10.1007/978-3-319-57852-1

Mitchell, N. C., Masson, D. G., Watts, A. B., Gee, M. J., and Urgeles, R. (2002). The Morphology of the Submarine Flanks of Volcanic Ocean Islands: A Comparative Study of the Canary and Hawaiian Hotspot Islands. *J. Volcanol. Geotherm. Res.* 115 (1-2), 83–107. doi:10.1016/S0377-0273(01)00310-9

Mitchell, N. C. (2001). Transition from Circular to Stellate Forms of Submarine Volcanoes. *J. Geophys. Res.* 106, 1987–2003. doi:10.1029/2000JB900263

Mittelstaedt, E., Ito, G., and Behn, M. D. (2008). Mid-Ocean Ridge Jumps Associated with Hotspot Magmatism. *Earth Planet. Sci. Lett.* 266, 256–270. doi:10.1016/j.epsl.2007.10.055

Morgan, W. J. (1971). Convection Plumes in the Lower Mantle. *Nature* 230, 42–43. doi:10.1038/230042a0

Nakamura, K. (1977). Volcanoes as Possible Indicators of Tectonic Stress Orientation - Principle and Proposal. *J. Volcanology Geothermal Res.* 2, 1–16. doi:10.1016/0377-0273(77)90012-9

Regelous, M., Hofmann, A. W., Abouchami, W., and Galer, S. J. G. (2003). Geochemistry of Lavas from the Emperor Seamounts, and the Geochemical Evolution of Hawaiian Magmatism from 85 to 42 Ma. *J. Petrol.* 44 (1), 113–140. doi:10.1093/petrology/44.1.113

Resing, J. A., Rubin, K. H., Embley, R. W., Lupton, J. E., Baker, E. T., Dziak, R. P., et al. (2011). Active Submarine Eruption of Boninite in the Northeastern Lau Basin. *Nat. Geosci* 4, 799–806. doi:10.1038/NGEO1275

Riley, S. J., DeGloria, S. D., and Elliot, R. (1999). Index that Quantifies Topographic Heterogeneity. *Intermountain J. Sci.* 5 (1-4), 23–27.

Romer, R. H. W., Beier, C., Haase, K. M., and Hübscher, C. (2018). Correlated Changes between Volcanic Structures and Magma Composition in the Faial Volcanic System, Azores. *Front. Earth Sci.* 6, 78. doi:10.3389/feart.2018.00078

Romer, R. H. W., Beier, C., Haase, K. M., Klügel, A., and Hamelin, C. (2019). Progressive Changes in Magma Transport at the Active Serreta Ridge, Azores. *Geochem. Geophys. Geosyst.* 20 (11), 5394–5414. doi:10.1029/2019GC008562

Somoza, L., González, F. J., Barker, S. J., Madureira, P., Medialdea, T., de Ignacio, C., et al. (2017). Evolution of Submarine Eruptive Activity during the 2011-2012 E L H Ierro Event as Documented by Hydroacoustic Images and Remotely Operated Vehicle Observations. *Geochem. Geophys. Geosyst.* 18, 3109–3137. doi:10.1002/2016GC006733

Staudigel, H., and Schmincke, H.-U. (1984). The Pliocene Seamount Series of la Palma/Canary Islands. *J. Geophys. Res.* 89 (B13), 11195–11215. doi:10.1029/JB089iB13p11195

Storey, M., Pedersen, A. K., Stecher, O., Bernstein, S., Larsen, H. C., Larsen, L. M., et al. (2004). Long-Lived Postbreakup Magmatism Along the East Greenland Margin: Evidence for Shallow-Mantle Metasomatism by the Iceland Plume. *Geology* 32 (2), 173–176. doi:10.1130/G19889.1

Torsvik, T. H., Mosar, J., and Eide, E. A. (2001). Cretaceous–Tertiary Geodynamics: A NorthAtlantic Exercise. *Geophys. J. Int.* 146 (3), 850–866. doi:10.1046/j.0956-540x.2001.01511.x

Voss, M., Schmidt-Aursch, M. C., and Jokat, W. (2009). Variations in Magmatic Processes Along the East Greenland Volcanic Margin. *Geophys. J. Int.* 177 (2), 755–782. doi:10.1111/j.1365-246X.2009.04077.x

Wessel, P. (1997). Sizes and Ages of Seamounts Using Remote Sensing: Implications for Intraplate Volcanism. *Science* 277, 802–805. doi:10.1126/science.277.5327.802

White, J. D. L., McPhie, J., and Soule, S. A. (2015). "Submarine Lavas and Hyaloclastite," in *The Encyclopedia of Volcanoes*. Editor H. Sigurdsson (London: Elsevier), 363–375. doi:10.1016/b978-0-12-385938-9.00019-5

Conflict of Interest: The authors declare that the research was conducted in the absence of any commercial or financial relationships that could be construed as a potential conflict of interest.

Publisher's Note: All claims expressed in this article are solely those of the authors and do not necessarily represent those of their affiliated organizations, or those of the publisher, the editors, and the reviewers. Any product that may be evaluated in this article, or claim that may be made by its manufacturer, is not guaranteed or endorsed by the publisher.

Copyright © 2021 Unger Moreno, Thal, Bach, Beier and Haase. This is an open-access article distributed under the terms of the Creative Commons Attribution License (CC BY). The use, distribution or reproduction in other forums is permitted, provided the original author(s) and the copyright owner(s) are credited and that the original publication in this journal is cited, in accordance with accepted academic practice. No use, distribution or reproduction is permitted which does not comply with these terms.